JOURNAL OF CHEMICAL INFORMATION AND MODELING

Article

pubs.acs.org/jcim

# Insight into the Allosteric Inhibition of Abl Kinase

Anna Lucia Fallacara,[†,‡] Cristina Tintori,[†] Marco Radi,[†,§] Silvia Schenone,[∥] and Maurizio Botta*[,†,⊥]

[†]Dipartimento di Biotecnologie, Chimica e Farmacia, Università degli Studi di Siena, Via Aldo Moro 2, 53100 Siena, Siena, Italy

[‡]Dipartimento di Chimica e Tecnologie Farmaceutiche, Sapienza Università di Roma, Piazzale Aldo Moro 5, 00185 Roma, Roma, Italy

[§]Dipartimento di Farmacia, Università degli Studi di Parma, Viale delle Scienze, 27/A, 43124 Parma, Parma, Italy

[∥]Dipartimento di Farmacia, Università degli Studi di Genova, Viale Benedetto XV, 3, 16132 Genova, Genova, Italy

[⊥] Sbarro Institute for Cancer Research and Molecular Medicine, Center for Biotechnology, College of Science and Technology, Temple University, BioLife Science Building, Suite 333, 1900 N 12th Street, Philadelphia, Pennsylvania 19122, United States

**ABSTRACT:** Abl kinase inhibitors targeting the ATP binding pocket are currently used as a front-line therapy for the treatment of chronic myelogenous leukemia (CML), but their use has significant limitation because of the development of drug resistance (especially due to the T315I mutation). Two compounds (GNF-2 and BO1) have been found able to inhibit the Abl activity through a peculiar mechanism of action. Particularly, GNF-2 acts as allosteric inhibitor against Bcr-Abl wild type (wt), but it has no activity against the gatekeeper mutant T315I. Its activity against the last mutant reappears when used together with an ATP-competitive inhibitor such as Imatinib or Nilotinib. A crystal structure of GNF-2 bound to the Abl myristoyl pocket (MP) has been released. On the contrary, BO1 shows an ATP-competitive/mixed mechanism of action against the wt, while it acts as an allosteric inhibitor against T315I. In order to better understand the mechanism of Abl allosteric inhibition, MD simulations and MM/GBSA analysis were performed on Abl wt and T315I in complex with GNF-2 and BO1, and the results were compared to those found for the natural myristoyl ligand. Similarly to that observed for the myristoyl group, the binding of an allosteric inhibitor to the MP promotes the formation of a compact and inhibited conformation of the wt protein, characterized by the stabilization of the intramolecular interactions that occur between SH2-SH3 and kinase domains. Conversely, an overall higher flexibility was observed with the Abl T315I mutant, especially in the case of GNF-2. Our analysis highlighted differences in the dynamic behavior of GNF-2 and BO1 which could explain the different biological profiles of the two allosteric inhibitors against the T315I mutant.

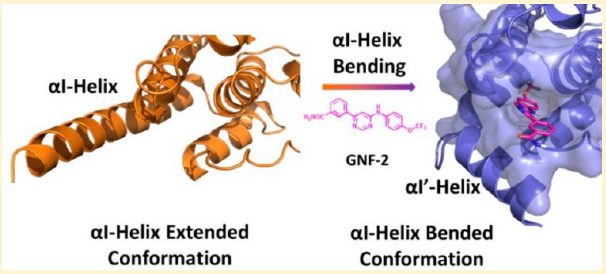


## INTRODUCTION

Chronic myelogenous leukemia (CML) is an hematological disorder characterized by an overproliferation of myeloid cells. The hallmark of CML is the presence of the chimeric Philadelphia Chromosome which derives from a reciprocal translocation between the chromosome 22 and chromosome 9.[1] This translocation causes the fusion of the Breakpoint Cluster Region from Ch 22 to the Abl gene on Ch 9. The hybrid gene encodes for an oncogenic protein (Bcr-Abl) endowed with deregulated tyrosine kinase activity. Today the front-line therapy for the treatment of CML consists of the use of Imatinib (IM or Gleevec, Figure 1),[2] an ATP-competitive inhibitor approved from FDA in 2001. However, many patients eventually develop resistance, frequently associated with mutations in the Bcr-Abl kinase domain.[3] In particular, the most troublesome mutation, consisting of the replacement of Thr315 with an Ile, occurs in the ATP binding site and confers resistance to almost all the ATP-competitive inhibitors.[4,5] Preclinical and clinical studies showed that ATP-competitive inhibitors BMS-35825 (Dasatinib),[6] AP23464,[7] and PD166326[8] inhibit Bcr-Abl more efficiently than IM and overcome resistance caused by most mutations, with the notable exception of T315I. Optimization of CML treatment remains an area of active research, and the development of new drugs targeting the T315I mutant is therefore a major challenge in CML therapy.

c-Abl is a tyrosine kinase that has been implicated in the process of cell differentiation, division, adhesion, and stress response. The kinase core of the c-Abl protein has a domain organization similar to that of the Src family kinases, with sequential Src homology SH3 and SH2 domains, an SH2/Kinase linker, and a bilobed kinase domain (Figure 2). This core is flanked by an N-terminal "cap" (N-cap) region with a signal sequence for myristoylation, which has an important role in regulation of kinase activity. The N-cap is about 80 amino acids in length and is myristoylated on Gly2.[9] The X-ray structure of the myristate bound form of c-Abl revealed that the myristic acid group binds a deep hydrophobic pocket in the C-terminal lobe (C-lobe) of the kinase domain.[9] The binding of

**Received:** January 29, 2014
**Published:** April 30, 2014

   dx.doi.org/10.1021/ci500060k | J. Chem. Inf. Model. 2014, 54, 1325−1338

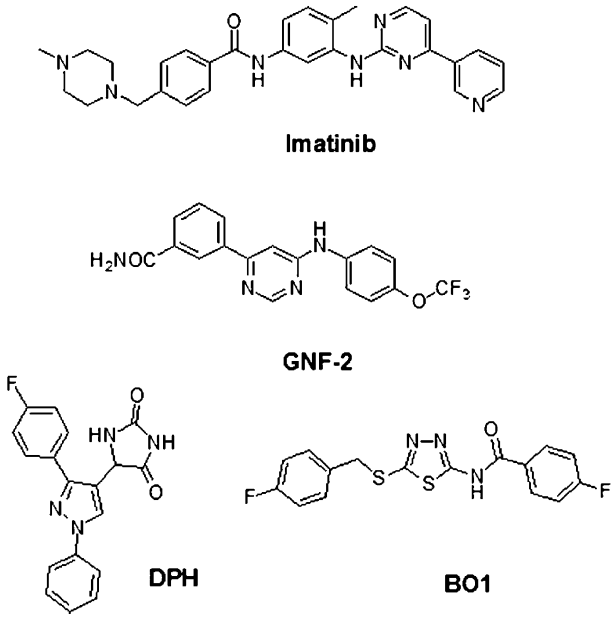


**Figure 1. 2D** structure of Imatinib (IM), GNF-2, DPH, and BO1 compounds.

the myristoyl group into this pocket (MP) is involved in the modulation of an autoinhibition mechanism of c-Abl. The main feature of this allosteric inhibition is the bending of the C-terminal αI-helix which allows the formation of a compact and inhibited conformation of the protein, which is stabilized by docking of the SH3 and SH2 domains onto the Abl kinase domain. The interaction of the myristoylated N-cap with the C-lobe is critical for the maintenance of the autoinhibition state, as mutation of the myristoylation signal sequence results in a highly active kinase.[10] Interestingly, small molecules that bind to the MP pocket also modulate kinase activity, supporting a connection between this allosteric pocket and the kinase active site.[11−13]

In this regard, a cocrystal structure of Abl in complex with the allosteric inhibitor GNF-2 has been solved.[14] This represents the first structure of an allosteric inhibitor bound to the myristoyl binding site of Bcr-Abl. The biological behavior of GNF-2 is of great interest because this compound has been shown to inhibit the wild type enzyme, but it failed to inhibit activity of mutated Bcr-Abl carrying the T315I mutation.[11−13] Its activity reappears when GNF-2 is used together with an ATP-competitive inhibitor such as Imatinib or Nilotinib.[11−13] In the last years, GNF-2 analogues were developed, and some of them have been demonstrated to synergize with Dasatinib against the T315I mutant,[15] but none is currently in clinical trials. On the other hand, a small-molecule c-Abl kinase activator that binds to the myristoyl binding site (5-(1,3-diaryl-1H-pyrazol-4-yl)hydantoin or DPH) has been recently discovered by a high-throughput screening campaign.[16] Differently from GNF-2, DPH stimulates c-Abl activation by preventing the formation of the bent conformation of the αI-helix through steric hindrance. The identification of DPH and other c-Abl activators[17] targeting the myristoyl pocket provides very valuable tools for studying the c-Abl mechanism of allosteric inhibition. Indeed, myristate ligands that bind but do not bend αI-helix are allosteric agonists of c-Abl kinase, and their c-Abl activation mechanism has been confirmed in a biochemical assay.[17] Vice versa, myristate ligands that bend αI-helix, such as GNF-2, are functional antagonists. Remarkably, because of the incidence of resistance to IM in advanced CML, many efforts are underway to find new compounds that address this challenge by acting as allosteric inhibitors of Bcr-Abl, and a new direct binding assay has been developed which exclusively detects the binding of ligands to the myristate pocket of Abl.[18]

In this context, our research group has recently identified a family of 1,3,4-thiadiazole derivatives as promising inhibitors of Bcr-Abl.[19] The lead compound BO1 (Figure 1) showed an interesting inhibitory activity on murine myeloid clones transduced with IM-sensitive or resistant Bcr-Abl.[19] Kinetic studies showed that this inhibitor acts on Abl wt and T315I with two different mechanisms of action: it was shown to be an ATP-competitive/mixed inhibitor of Abl wt and a purely noncompetitive-ATP inhibitor in the case of Abl T315I.[19] In this work, molecular modeling studies have been conducted in order to elucidate from a theoretical point of view the biological behavior of c-Abl allosteric inhibitors. We focused our studies on the known compounds GNF-2 and BO1. At first, docking simulations of the two inhibitors were performed on Abl wt and T315I within both ATP and myristoyl binding sites. Subsequently, molecular dynamic (MD) simulations[20] were applied to optimize the protein systems and to calculate the free energy of binding through the use of the MM/GBSA.[21,22] Results allowed understanding of the mechanism by which GNF-2 and BO1 inhibited Abl wt and T315I.

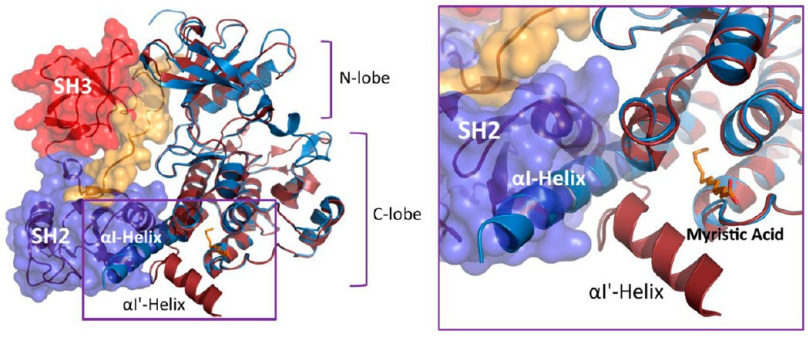


**Figure 2.** *Left.* Overview of c-Abl structure. *Right.* Focus on the contacts between SH2 (purple) and the C-lobe of kinase domain (blue/brown). The Abl structure characterized by the αI-helix in an extended conformation (light blue, PDB code 3IK3) was overlapped with the structure of the protein in complex with the myristoyl (brown, PDB code 1OPK). The comparison suggests a myristoyl switching mechanism: the binding of the myristoyl group into the pocket causes the bending of the αI-helix and the subsequent approach of SH2 domain to the kinase domain.

## METHODS

**Proteins Preparation.** The crystal structure of c-Abl$^{83-531}$ wt (including kinase, SH2 and SH3 domains) in complex with the myristic acid was retrieved from the Protein Data Bank (PDB code: 1OPK).[9] After removal of the bound ligand, the protein was prepared by using the Protein Preparation Wizard workflow,[23] from Schrodinger Suite. In particular all water molecules were deleted, hydrogen atoms were added, and partial charges were assigned. In addition, the ionization and tautomeric states of His, Asp, Glu, Arg, and Lys were adjusted to match a pH of 7.4. Next, optimization of the hydrogen-bonding network was obtained by reorienting hydroxyl and thiol groups, amide groups of Asn and Gln, and His ring. Finally, the system was refined by running a restrained minimization (OPLS2005 force field) which was stopped when RMSD of heavy atoms reached 0.30 Å, the specified limit by default.

The three-dimensional structure of c-Abl$^{83-531}$ T315I was prepared starting from the wt structure by mutating the Thr315 into an Ile. The protein system was then prepared according to the procedure already described for the wt enzyme. Once prepared, the two protein structures were used for docking studies.

**Ligand Preparation.** Compounds BO1 and GNF-2 were drawn and minimized using Maestro 9.2[24] and Macromodel[25] (Schrödinger suite), respectively. Furthermore, Ligprep[26] was used to predict ionization and tautomeric states for the ligands using a pH of 7 ± 1.

**Docking Studies.** Docking simulations were performed using the Glide program[27] within both MP and ATP binding sites of Abl wt and T315I. The prepared protein systems were used to generate the receptor grids, and no scaling was done for van der Waals radii of nonpolar receptor atoms. A grid box of default size was centered on the X-ray ligand. No constraints were included during grid generation, while the rotation of the hydroxyl groups was allowed. After grid preparation, compounds were flexibly docked and scored using the Glide standard-precision (SP) mode, treating the proteins as rigid. Docking experiments were performed using 0.80 factor to scale VdW radii of the nonpolar ligand atoms with partial atomic charge less than 0.15.

**MD Simulations.** Molecular dynamics simulations were performed starting from the best docking poses of BO1 and GNF-2 within the MP and ATP binding sites of both Abl wt and T315I and according to a procedure already reported.[28] General Amber Force Field (GAFF)[29] parameters were assigned to ligands, while partial charges were calculated using the AM1-BCC method as implemented in the Antechamber[30] suite of AMBER11. The standard AMBER11 ff99SB force field for bio-organic systems was used to describe the protein parameters. Each complex was placed in an octahedron box of TIP3P water molecules, and an appropriate number of counterions (9 Na+ ions) was added. The distance between the box walls and the protein was set to 10 Å. Before MD simulations, two steps of energy minimization were performed to remove bad contacts. In the first stage, the protein was kept fixed with a constraint of 500 kcal/mol, and only the water molecules were minimized. In the second stage, the entire system was minimized applying a constraint of 10 kcal/mol on the $\alpha$-carbon. The two minimization stages consisted of 5000 steps in which the first 1000 were steepest descent and the last were conjugate gradient. MD trajectories were run using the minimized structures as a starting point. Constant volume simulations were performed for 500 ps, during which the temperature was raised from 0 to 300 K using the Langevin dynamics method. Then 1500 ps of constant-pressure MD simulations were performed at 300 K in three steps of 500 ps each. During these steps a decreasing harmonic force constraint of 10, 5, and 1 kcal/mol·Å was applied, respectively. Finally, a 12 ns MD simulations for the endogenous ligand and 30 ns MD simulation for GNF-2 and BO1 without restraints were run at constant temperature of 300 K and a constant pressure of 1 atm. During the simulations, the Particle Mesh Ewald method was employed to calculate the long-range electrostatic interactions. A 10-Å cutoff value was used for the nonbonded interactions, and a time step of 2 fs was used for the simulations.

**Analysis of MD Trajectories.** The module Ptraj implemented in AMBER11 was used to analyze trajectories. In particular, the root-mean-square deviation (RMSD) and the root-mean-square fluctuation (RMSFs) were calculated for the $\alpha$-carbons of each residue on the production stage. During the simulation, the hydrogen bonds between SH2 and kinase domains as well as kinase domain and ligands were detected when the acceptor−donor atom distance was lower than 3.5 Å and the occupancy was more than 10% in the investigated time period.

**MM/GBSA Analysis.** The MM/GBSA approach was used to evaluate the binding free energy between the preferred poses of ligands (BO1 and GNF-2) and the proteins. This method estimates the $\Delta G_{bind}$ as the difference in free energy between the complex (PL), the ligand (L), and the receptor (P).

$$\Delta G_{bind} = G(PL) - G(P) - G(L) \quad (1)$$

Each binding free energy term in eq 1 was estimated from the following eq 2

$$\Delta G = \Delta G_{MM} + \Delta G_{sol} - T\Delta S \quad (2)$$

where $\Delta G_{MM}$ (molecular mechanics) is the gas phase energy and was calculated by eq 3 as sum of electrostatic and van der Waals interactions energies; $\Delta G_{solv}$ is the solvation free energy and was computed with eq 4, while the last term is the absolute temperature multiplied by the estimated entropy. The entropy term was considered negligible, and it was thus not calculated in this work being computationally expensive.

$$\Delta G_{MM} = \Delta G_{ele} + \Delta G_{vdW} \quad (3)$$

The solvation free energy was composed of polar and nonpolar contributions

$$\Delta G_{Sol} = \Delta G_{ele,sol} + \Delta G_{nonpol,sol} \quad (4)$$

where the polar part $\Delta G_{ele,sol}$ was calculated by solving the Poisson−Boltzmann (PB)[31] equation in the case of the MM/PBSA method or the generalized Born (GB)[32] model with the MM/GBSA. The nonpolar solvation was estimated using eq 5 by calculating the solvent accessible surface area (SASA) with the AMBER11 molurf module:

$$G_{nonpol} = \gamma^{*}SASA + b \quad (5)$$

In detail, SASA was determined by recursively approximating a sphere around each atom, starting from icosahedra (ICOSA method). The radius of the probe sphere used to calculate the SASA was set to 0.0. The surface tension proportionality constant $\gamma$, and the free energy of nonpolar solvation for a point


dx.doi.org/10.1021/ci500060k | J. Chem. Inf. Model. 2014, 54, 1325−1338

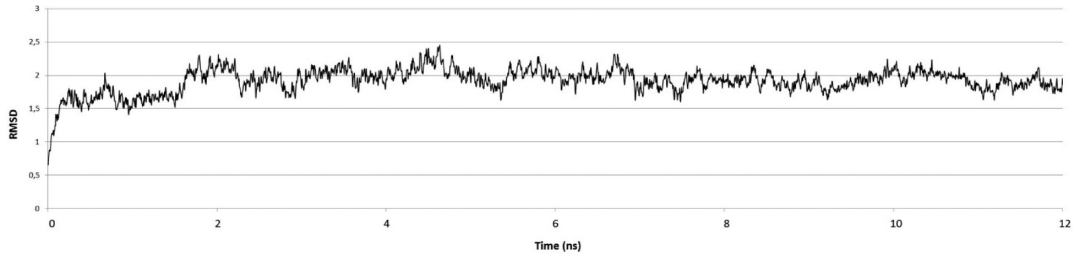


**Figure 3.** Time evolution of the root-mean-square deviations (RMSD calculated on C$\alpha$) of the myristoyl-Abl wt complex from the corresponding initial structure.

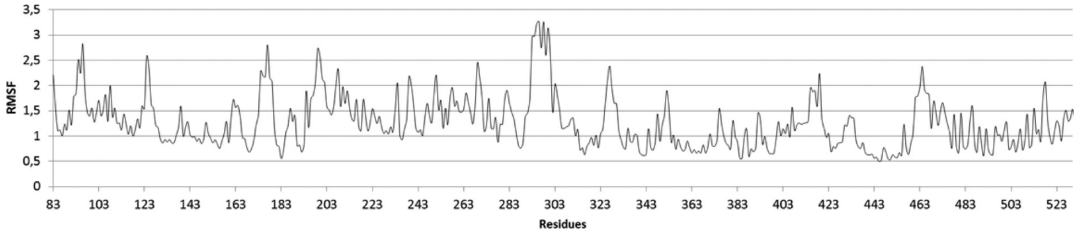


**Figure 4.** RMSF value of each residue calculated from the MD simulation on the myristoyl-Abl wt complex. The number of residues is reported in abscissa, while the RMSF expressed in Å is reported in ordinate.

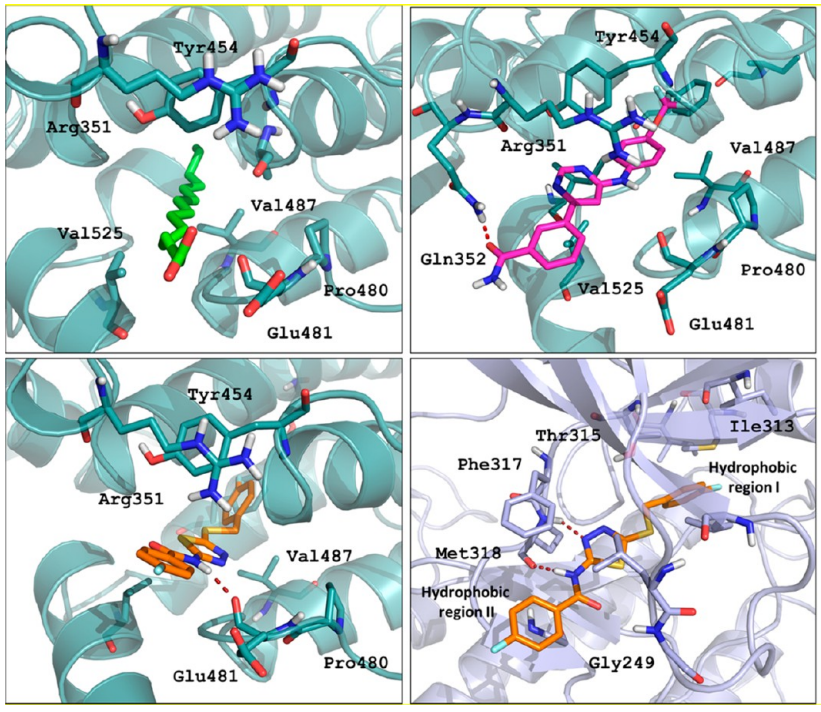


**Figure 5. A)** Binding mode of myristic acid in the MP (PDB code: 1OPK). B) Docking pose of GNF-2 in MP. C) Docking pose of BO1 in MP. D) Docking pose of BO1 within the ATP binding site of Abl wt. For reasons of clarity only a few residues were shown. All docking poses have been used as a starting point of MD simulations.

solute *b* were set to 0.0072 kcal/(mol Å$^2$) and 0.00 kcal/mol, respectively. Binding free energies were calculated on systems where water molecules used during the simulation were stripped off, with the exception of selected water molecules involved in interactions with the ligands. Only the complex PL was simulated, and the free energies of P and L were obtained from the same simulation by simply deleting the coordinates of the other species, as well as generally made. The last 6 ns of our simulations were regarded as stable and were used to extract 150 snapshots from each trajectory. The ligand-protein binding free energy ($\Delta G_{bind}$) for each snapshot was then estimated using eq 1. The MM-GBSA approach was also used to decompose the binding free energies into individual amino acid contributions in order to map the interactions that have a dominant role in the complexes formation (hot spot residues).

## RESULTS AND DISCUSSION

**Myristic Acid Binds c-Abl Stabilizing the Auto-inhibited Conformation.** The crystal structure of c-Abl wt bound by the myristic acid (PDB code 1OPK)[9] has been solved revealing the structural basis for the autoinhibition of Abl tyrosine kinase. The structure shows that the myristic acid is


dx.doi.org/10.1021/ci500060k | J. Chem. Inf. Model. 2014, 54, 1325−1338

buried in a deep pocket on the C-lobe of kinase domain, referred to as the myristoyl pocket (MP, Figure 3A). MP consists of hydrophobic residues belonging to the αE (Ala356, Val357, Val358, Leu359, Leu360), αH (Cys483, Pro484, Val487, Leu490), αF (Leu448, Ala452, Tyr454), and αI′ (Ile521, Val525, Leu529) helices. In order to identify the relevant residues for the ligand-protein interaction (hot spots) and to assess the theoretical protocol the system was computationally analyzed. With this purpose, a MD simulation has been performed to optimize the complex and to calculate the free energy of binding by an MM-GBSA analysis. The root-mean-square deviations (RMSDs) of the α-carbons were calculated throughout the simulation with respect to the starting structure to check whether the protein reached the equilibration state during the MD simulation. Results are graphically represented in Figure 4. An equilibrium plateau was reached after the first 2 ns, and the complex remained stable during the remaining simulation. Although the RMSD is a useful tool to analyze the dynamic behavior of the whole protein, we were also interested in determining which parts of the receptor were the most stable after ligand binding. Accordingly, the RMSFs of the α-carbons of each residues were calculated during the last 6 ns of simulation (Figure 5). We observed a high stability of the SH2 domain (residues 145−234), the SH2/SH3 linker (residues 133−144), the SH2/kinase linker (residues 231−253), and the C-lobe (residues 421−531), which also included the MP. Conversely, higher fluctuations were detected in the αC-helix which is located within the ATP binding site. Analysis of the time-dependent RMSD and RMSF fluctuations could provide only an initial and qualitative outlook of potential complex stability. The thermodynamic effect of ligand binding could be quantified more rigorously when the results of MD simulation are combined with the MM-GBSA analysis. Accordingly, a total of 150 frames were extracted from the last 6 ns of the MD trajectory and used for the following structural and energetic analysis. Overall, the total binding free energy predicted for the binding of myristic acid into the MP was found to be −32.45 kcal/mol. Next, in order to identify the key residues for the protein−ligand interaction, binding free energy decomposition at the atomic level was made to evaluate the contribution of each amino acid to the binding process (Table 1). The major favorable energy contributions originate predominantly from residues of hydrophobic character such as Leu359, Leu448, Ile451, Ala452, Val487, and Ile521 ($\Delta G_{bind}$ ← 1.5 kcal/mol). However, the residue for which we had the highest value of $\Delta G$ was the Arg351 ($\Delta G_{bind}$ = −3.77 kcal/mol), which was involved in apolar interaction with the carboxyl group of the fatty acid (Figure 6A). Consistently, a stable hydrogen-bond was found between Arg351 and the myristic acid with total occupancy higher than 50%. From a structural point of view, the binding of the myristoyl ligand to the C-lobe reorients the C-terminal αI-helix of the kinase domain and enables the assembling of the autoinhibited conformation of c-Abl by allowing the docking of the SH2 domain to the C-lobe. The effect of the myristoyl on the stability of these intramolecular interactions was studied by analyzing the binding free energy between the SH2-SH3 domains and the kinase domain after ligand binding. Estimation of the $\Delta G$ value between the two interacting domains obtained from the MM-GBSA calculation was −57.58 kcal/mol. The amino acids that gave a significant favorable contribution to the binding free energy between SH2-SH3 and kinase domains (namely hot-spots, $\Delta G_{bind}$ ←1 kcal/mol) are reported in Table 2. Most of the hot-spots identified are involved in polar interactions such as Glu117, Ser152, Arg153, Asn154, Glu157, Tyr158, Arg189, Arg194, and Arg239 from SH2/SH3 domains and Lys313, Asn393, His394, Phe512, Phe516, Glu513, Glu518, Ser519, Ser520, Asp523, and Glu526 from kinase domain (Tables 2-3, Figure 7). Furthermore, residues Tyr158, Tyr245, and Val247 from SH2 and SH3 domains were involved in hydrophobic contacts with Tyr283, Leu285, Lys313, Val357, Val358, and Tyr361 belonging to the kinase domain. According to mutagenesis studies[9] which demonstrated the crucial role of the residue Tyr158 for the correct positioning of the SH2 domain in the autoinhibited conformation, a favorable π−π interaction was observed in our study between Tyr158 and Tyr361, contributing to the total free energy of binding with an energy of −3.5 kcal/mol and −2.40, respectively (Table 2). Arg189 has also emerged as a crucial residue with a contribution of −5.16 kcal/mol. According to the hydrogen bonds analysis (Table 3), Arg189 established favorable polar contacts with Glu526 and Asp523.

**Table 1. Hot Spots Identified by Per Residue Decomposition Analysis for All Ligands in Both Abl wt and T315I Mutants[a]**

| | Abl wt | | | Abl T315I | | |
|---|---|---|---|---|---|---|
| res | Myr | GNF-2 | BO1 | GNF-2 | GNF-2+IM | BO1 |
| **Arg351** | −3.77 | −1.60 | | | −1.98 | −1.61 |
| **Ala356** | −1.03 | −1.07 | −1.03 | −1.50 | −1.15 | −1.19 |
| **Leu359** | −1.56 | −2.08 | −1.84 | | −1.57 | −1.69 |
| **Leu360** | −1.05 | −1.85 | −1.06 | | −1.88 | −1.23 |
| **Leu448** | −1.54 | −1.91 | −1.66 | | −1.15 | −1.18 |
| **Ile451** | −1.75 | −1.75 | | −2.19 | −1.91 | |
| **Ala452** | −1.89 | −1.48 | −1.39 | −1.27 | −1.49 | −1.56- |
| **Tyr454** | | −1.87 | −1.68 | 1.71 | −1.84 | −1.34 |
| **Glu481** | | −2.36 | −2.53 | | −1.05 | −2.11 |
| **Gly482** | | −1.11 | −1.49 | −1.45 | −1.10 | −1.58 |
| **Cys483** | −1.10 | −1.76 | −2.14 | −2.28 | −1.00 | −1.78 |
| **Val487** | −1.73 | −1.94 | −1.16 | | −1.03 | −1.80 |
| **Ile521** | −1.68 | −1.47 | | | −1.15 | - |
| **Val525** | −1.07 | −1.28 | −1.12 | −1.77 | | −1.16 |
| **Val525** | | −1.66 | −1.12 | −1.51 | | |
| **Leu529** | | −1.65 | −1.84 | −2.33 | −1.54 | −1.47 |

[a]Only residues with a $\Delta G$ value < −1 kcal/mol are reported.

**GNF-2 Stabilizes the Interactions between SH2 and Kinase Domains of Abl wt.** In order to study the mode of action of GNF-2 against Abl wt from a theoretical point of view, we applied to this ligand the computational protocol previously assessed for the myristoyl group. For comparison purposes, GNF-2 was docked within the myristoyl binding site of 1OPK after removal of the endogenous ligand. Docking simulation was carried out by means of the program Glide.[27] The reliability of the docking protocol was checked by comparing the modeled complex with the available crystal structure of GNF-2 bound to the MP of Abl wt (PDB code 3K5V).[12] The program perfectly reproduced the experimental binding mode of GNF-2 as demonstrated by the low root-mean-square deviation (RMSD) of 0.53 Å (calculated on all the ligand heavy atoms). GNF-2 adopts an extended trans conformation within the MP (Figure 3B) with the *p*-trifluoromethoxy phenyl group oriented toward the bottom of the pocket where established hydrophobic interactions with residues Leu359, Ile451, Val487, Val525, Ala356, and Cys483. Hydrophobic contacts were also found between the central pyrimidine core of GNF-2 and the amino acids Leu529 and Tyr454. Furthermore, the benzamide


dx.doi.org/10.1021/ci500060k | J. Chem. Inf. Model. 2014, 54, 1325−1338

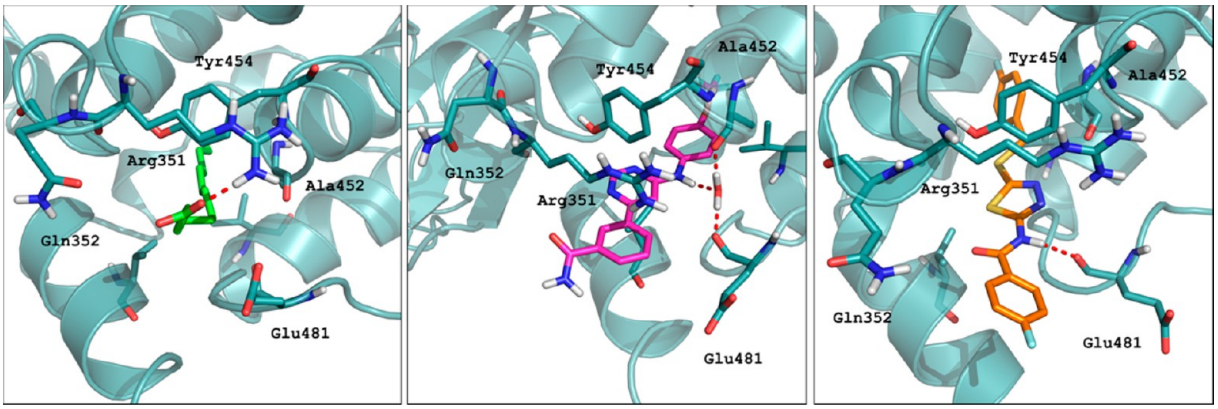


**Figure 6.** Results of MD simulations. A) Last frame of MD of myristic acid within MP of Abl wt. The ligand forms a hydrogen bond with Arg351. B) Last frame of MD simulation of GNF-2 within MP of Abl wt. A molecule of water forms a bridge between GNF-2 and the main chain carbonyls of Ala452 and Glu481. C) Last frame of MD simulation of BO1 bound to MP of Abl wt. A stable hydrogen bond was found during the trajectory.

**Table 2. Hot Spots Identified between SH3-SH2 and Kinase Domain for All the Simulations**[a]

| | Abl wt | | | Abl T315I | | |
|---|---|---|---|---|---|---|
| res | Myr | GNF-2 | BO1 | GNF-2 | GNF-2+IM | BO1 |
| **Asp96** | | −1.76 | | | | −1.10 |
| **Glu117** | −1.15 | −1.27 | −1.26 | | −1.27 | −1.69 |
| **Ser152** | | −1.78 | | −1.06 | −1.16 | |
| **Arg153** | | | −1.26 | | | −3.02 |
| **Asn154** | −1.14 | −1.37 | −1.40 | | | −1.38 |
| **Glu157** | −1.4 | −1.74 | −1.40 | −1.37 | −1.61 | −1.4 |
| **Tyr158** | −3.50 | −4.18 | −3.55 | −3.50 | −3.69 | −3.68 |
| **Arg189** | −5.16 | −5.89 | −5.38 | −4.68 | −5.75 | −5.18 |
| **Arg194** | −3.13 | −3.50 | −3.15 | | −2.02 | −5.87 |
| **Tyr245** | −4.68 | −4.51 | −4.54 | −4.60 | −4.60 | −4.30 |
| **Val247** | −1.74 | −2.18 | −2.32 | | −2.30 | −2.10 |
| **Lys253** | −1.13 | −1.22 | −1.44 | | | 1.87 |
| **Trp254** | −1.29 | | −2.03 | | | |
| **Lys282** | | −2.48 | | | | −1.83 |
| **Tyr283** | −1.28 | −2.75 | −2.73 | −2.58 | 2.19 | −2.80 |
| **Lys313** | −1.20 | −1.85 | −1.94 | | −2.12 | −1.47 |
| **His314** | −1.58 | −1.37 | −1.20 | −1.36 | −1.35 | −1.36 |
| **Pro315** | | −1.88 | −2.31 | | −1.80 | −1.71 |
| **Val357** | −2.69 | −2.24 | −1.06 | −2.56 | −2.30 | −2.30 |
| **Val358** | −1.37 | −1.27 | | | −1.32 | −1.31 |
| **Tyr361** | −2.40 | −2.48 | −2.50 | −2.48 | −2.71 | −2.79 |
| **His394** | −1.47 | −1.41 | −1.44 | −1.53 | −1.37 | −1.31 |
| **Phe512** | −1.95 | −2.10 | −1.34 | | −1.01 | −1.30 |
| **Phe516** | | −1.12 | −1.34 | | −1.09 | −1.03 |
| **Glu518** | −1.72 | −2.28 | −2.14 | | | −1.27 |
| **Ser520** | −2.53 | −1.85 | −1.78 | −1.35 | −1.54 | −1.35 |
| **Asp523** | | −1.40 | −1.44 | −1.73 | −2.42 | |
| **Glu526** | 1.02 | −2.01 | −1.27 | −1.73 | −1.87 | |

[a]Only residues with an energy < −1 kcal/mol are reported.

substituent established a hydrogen-bonding interaction with the Gln352 side chain. After docking, a 30 ns MD simulation has been performed on the complex according to the procedure previously described for the myristic acid. Figure 8 shows the RMSDs of the $\alpha$-carbons throughout the simulation with respect to the starting structure (black line). Ten nanoseconds was the time required by the complex to reach the stability that was kept for the remaining time of simulation. The RMSFs profile for GNF-2 (Figure 9 upper, black line) resulted in being quite similar to the one of the myristoyl group. The observed low fluctuations suggested an overall stability of the system. Moving to the MM-GBSA analysis, the last stage of simulation was considered to extract 150 snapshots which were used to calculate the ligand−receptor binding free energy. Results are shown in Table 4.

The total free energy for the binding of GNF-2 to Abl wt was −34.73 kcal/mol when MM-GBSA was applied without considering water molecules. However, MD movie analysis highlighted a favorable interaction between the ligand aniline NH and a water molecule which was observed during most part of the simulation (occupancy of 68%). This water molecule forms bridges between GNF-2 and the main chain carbonyls of Ala344 and Glu462 (Figure 6B). To quantitatively investigate the contribution of this water molecule to the binding free energy of GNF-2, 150 frames were again extracted from the MD run including the water molecule as part of the receptor. As expected, the total binding free energy was estimated to be −36.27 kcal/mol, about 2 kcal/mol higher than that found excluding the solvent. Remarkably, the water molecule selected from the dynamic is located exactly in the same position of a structural water found in the 3K5V crystal structure. To further investigate this aspect, molecular interaction fields (MIFs) were calculated for the binding site by means of the software Grid[33] using the water probe (OH2). MD results and Grid analysis were then combined together. Interestingly, a minimum grid point characterized by a significant favorable energy (−9.83 kcal/mol) was found near the water molecule involved in the binding of GNF-2 in both dynamics frame and 3K5V X-ray structure. Figure 10 shows one of the snapshots extracted from MD trajectory together with the region of minimum energy determined for the probe OH2 (dark red sphere) within the MP. Overall, these results highlighted that a water molecule plays a crucial role in mediating the interactions of GNF-2 with Abl wt. On the other hand, a per residue decomposition was carried out in order to estimate the contribution of each residue to the binding process (Table 1). The main contributions were of a hydrophobic nature and originate from almost the same residues involved in the binding of the myristoyl group (Leu359, Leu360, Ile451, Cys483, Val487, and Val525). Additionally, GNF-2 also established hydrophobic contacts with amino acids Ile451 and Tyr454. Differently from the myristoyl group, no polar contacts were found between GNF-2 and Arg351. The $\Delta G$ value of −1.60 kcal/mol that emerged from decomposition analysis for such an amino acid was due to


dx.doi.org/10.1021/ci500060k | J. Chem. Inf. Model. 2014, 54, 1325−1338

Table 3. Hydrogen Bonds Occupancy for All Ligands in Both Abl wt and T315I Mutants[a]

| SH2-SH3 domains | | kinase domain | | Abl wt | | | Abl T315I | | |
|---|---|---|---|---|---|---|---|---|---|
| res | group | res | group | Myr in MP (% occupancy) | GNF-2 in MP (% occupancy) | BO1 in MP (% occupancy) | GNF-2 (% occupancy) | GNF-2+IM (% occupancy) | BO1 (% occupancy) |
| **Asp96** | O | **Arg282** | H | | | | | | 35 |
| **Ser93** | HG | **Val247** | O | | 24 | 26 | | 36 | 35 |
| **Glu117** | OE1 | **Lys313** | HZ1 | 30 | | | | 25 | 30 |
| **Glu117** | OE2 | **Lys313** | HZ3 | 25 | 15 | 31 | 27 | 21 | 23 |
| **Glu117** | OE1 | **Lys313** | HZ3 | 18 | 11 | 22 | 20 | 20 | 21 |
| **Glu117** | OE1 | **Lys313** | HZ2 | 13 | 40 | | | 15 | 18 |
| **Glu117** | OE2 | **Lys313** | HZ1 | 11 | 28 | 15 | 24 | | 16 |
| **Asn154** | HD21 | **Phe512** | O | 52 | 55 | 41 | 46 | | 58 |
| **Arg153** | HH12 | **Glu518** | OE1 | 23 | | 14 | | 12 | 38 |
| **Arg239** | HH11 | **Asn393** | OD1 | | 71 | | | | 33 |
| **Tyr158** | HH | **His394** | ND1 | 64 | 73 | 58 | 38 | 73 | 77 |
| **Tyr158** | HH | **Asn393** | OD1 | 12 | 12 | | 48 | 70 | 43 |
| **Tyr158** | HH | **Asn393** | O | | 10 | 12 | | | 14 |
| **Glu157** | OE2 | **Ser520** | HG | 77 | 50 | 64 | 52 | 45 | 45 |
| **Glu157** | OE1 | **Ser520** | HG | 22 | 29 | 53 | 39 | | 41 |
| **Arg189** | HH22 | **Asp523** | OD1 | | 16 | 16 | | | 24 |
| **Arg189** | HH21 | **Asp523** | OD2 | 10 | 35 | 12 | 21 | 56 | 15 |
| **Arg189** | HH21 | **Asp523** | OD1 | | 10 | 12 | 41 | 36 | 15 |
| **Ser152** | HG | **Glu513** | OE2 | 35 | 25 | 52 | 44 | 15 | 86 |
| **Ser152** | HG | **Glu513** | OE1 | 35 | 25 | 41 | 31 | 11 | |
| **Arg189** | HH21 | **Glu526** | OE2 | 23 | 10 | 32 | 11 | | 15 |
| **Arg194** | HH11 | **Glu518** | OE1 | 23 | 30 | | | | 40 |
| **Arg194** | HH22 | **Glu518** | OE2 | 21 | 43 | 13 | | | 64 |
| **Arg153** | HH12 | **Ser519** | O | 18 | | 14 | | 10 | |
| **Arg153** | HH11 | **Ser519** | O | 16 | 21 | 12 | 16 | 15 | 12 |
| **Arg189** | HE | **Glu526** | OE1 | 15 | 12 | | 38 | 51 | |
| **Arg189** | HH22 | **Glu526** | OE2 | 25 | 30 | 22 | | 36 | 13 |
| **Arg189** | HH21 | **Glu526** | OE1 | 22 | 16 | 10 | 10 | 13 | 12 |

[a]Only residues with occupancy >10% are reported.

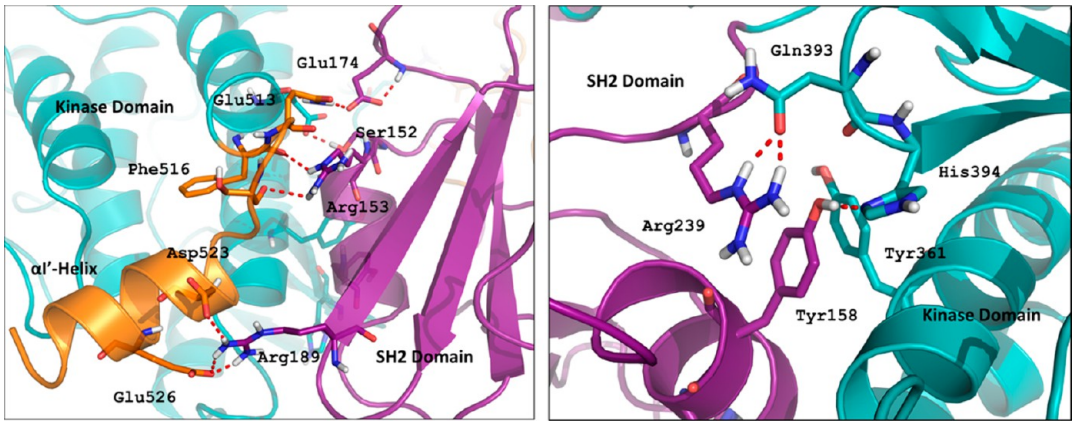


**Figure 7.** *Left.* Overview of the contacts at the interface between SH2 and kinase domains. The main residues are shown in sticks. *Right.* $\pi-\pi$ interaction between Tyr158 and Tyr361 belong to SH2 and kinase domain, respectively. These two residues have been identified as hot spots, contributing to stabilize the compact/autoinhibited conformation.

a $\pi-\pi$ interaction between the guanidine group of the residue and the benzamide of GNF-2 (Figure 6B). Finally, a weak hydrogen bond was found between GNF-2 and Gln352 (15% occupancy), but such interaction at the entrance of the pocket was occasional because of the high flexibility of both GNF-2 and all residues side chains in that solvent exposed region. Next, as for myristoyl ligand, the binding free energy between SH2 and kinase domain was calculated to investigate the effect of the GNF-2 binding on the stabilization of the autoinhibited conformation of the protein. Results are summarized in Table 5. From this analysis, the binding of GNF-2 into the MP was associated with the stabilization of the Abl compact conformation as demonstrated by the value of the binding free energy between SH2/SH3 and kinase domains, comparable to that found with the myristoyl endogenous ligand (−60.73 kcal/mol versus −57.58 kcal/mol). As described above, total energy was decomposed on a per residue contribution, and hydrogen bond occupancies were monitored


dx.doi.org/10.1021/ci500060k | J. Chem. Inf. Model. 2014, 54, 1325−1338

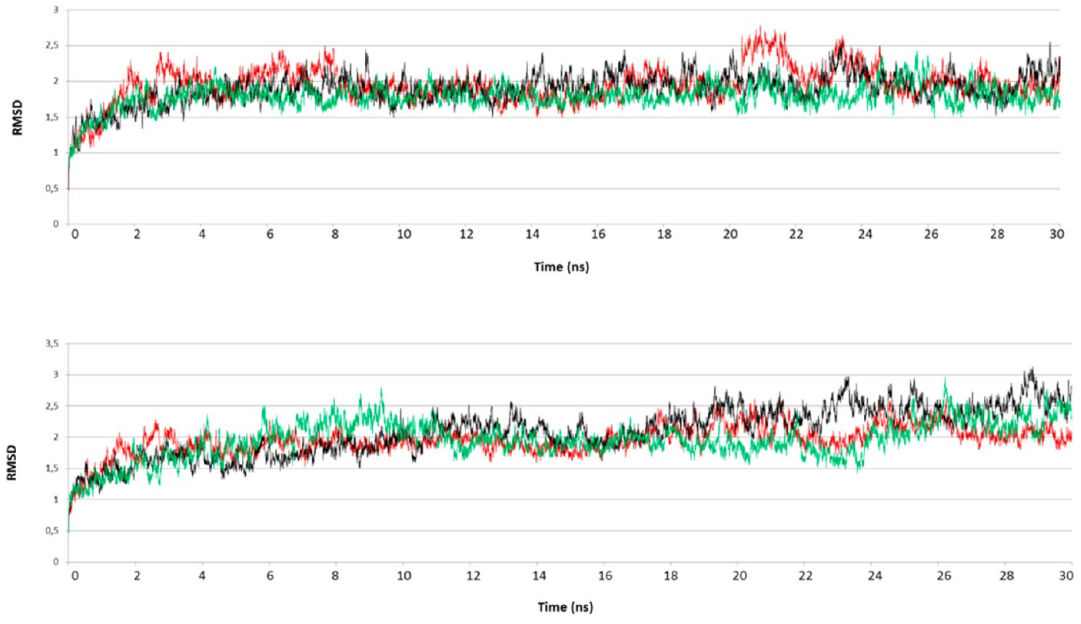


**Figure 8.** Time evolution of the RMSD values (calculated on $\alpha$-carbons) of all the complexes analyzed by MD simulations. The upper graph shows the plots obtained by MD simulations on the GNF-2 ligand bound to MP of Abl wt (black line), MP of the T315I mutant (red line), and MP of the T315I mutant with the concurrent binding of Imatinib within the ATP binding site (green line). The bottom graph shows the plots obtained by MD simulations on the BO1 ligand bound to MP of Abl wt (black line), the ATP binding site of Abl wt (green line), and MP of the T315I mutant (red line).

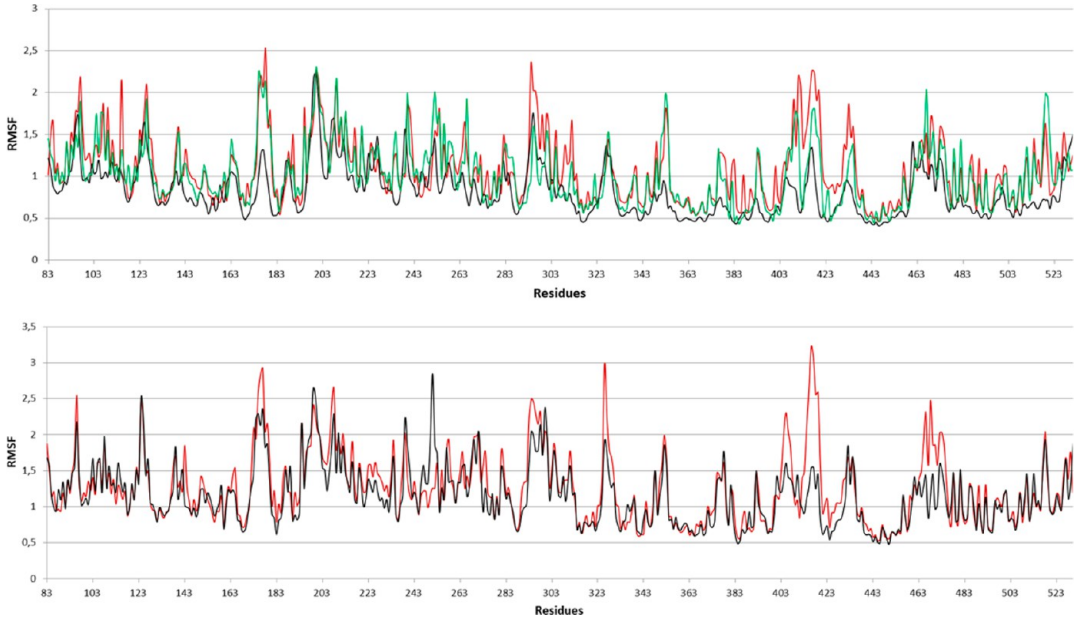


**Figure 9.** RMSF value of each residue calculated from the MD simulation on all the studied complexes. The upper graph shows the plots obtained from MD simulations on GNF-2 bound to MP of Abl wt (black line), MP of the T315I mutant (red line), and MP of the T315I mutant with the concurrent binding of Imatinib within the ATP binding site (green line). The bottom graph shows the plots obtained from MD simulations on BO1 bound to MP of Abl wt (black line) and MP of the T315I mutant (red line). The number of residues is reported in abscissa, while the RMSF expressed in Å is reported in ordinate.

**Table 4. Binding Free Energies Calculated by MM-GBSA for the Ligands under Study**

| compd | MP wt $\Delta G$ (kcal/mol) | ATP site wt $\Delta G$ (kcal/mol) | MP T315I $\Delta G$ (kcal/mol) |
|---|---|---|---|
| **Myr** | −32.45 ± 2.54 | | |
| **GNF-2** | −34.73 ± 2.23/−36.27 ± 2.71 | | −27.08 ± 1.04 |
| **GNF-2+IM** | | | 32.26 ± 2.36 |
| **BO-01** | −33.72 ± 1.47 | −36.49 ± 2.23 | −32.76 ± 2.33 |


dx.doi.org/10.1021/ci500060k | J. Chem. Inf. Model. 2014, 54, 1325−1338

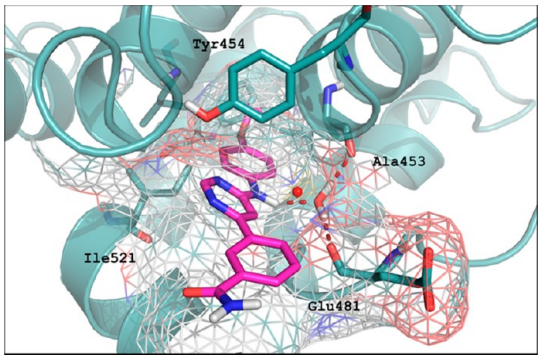


**Figure 10.** Snapshot from MD simulation of GNF-2 bound to the MP of Abl wt. A water bridge involving GNF-2, Glu481, and Ala452 stabilized the complex. GRID analysis was performed, and the most favorable interaction point determined for the probe OH2 (water, dark red sphere) resulted located in the close proximity of water molecule.

**Table 5. ΔG Values Calculated between SH2 and Kinase Domain of Abl**

| compd | MP wt ΔG (kcal/mol) | MP T315I ΔG (kcal/mol) |
|---|---|---|
| **Myr** | −57.58 ± 2.75 | |
| **GNF-2** | −60.73 ± 2.28 | −42.10 ± 2.51 |
| **GNF-2+IM** | | −47.05 ± 2.98 |
| **BO1** | −58.40 ± 1.65 | −59.41 ± 2.18 |

throughout the simulations (Tables 2-3). The key residues driving the favorable interaction between kinase and SH2-SH3 domains (ΔG value < −2 kcal/mol) were found to be Tyr158, Arg189, Arg194, Tyr245, and Val247 from SH2-SH3 domains and Lys282, Tyr283, Val357, Tyr361, Phe512, Glu518, and Glu526 from kinase domain. Among them, Tyr245, Val247, Val357, Tyr361, Lys282, Tyr283, and Phe512 were mainly involved in hydrophobic interactions. Conversely, polar contacts were made by the other residues. Particularly, stable hydrogen bonds occur between Arg189 and both Glu526 and Asp523 as well as from Arg194 and Glu518. Interestingly, Tyr158 made $\pi-\pi$ interaction with Tyr361 but also established permanent hydrogen bonds with His394 and Asn393. Overall, results from our theoretical calculations highlighted a good stability of the complex between GNF-2 and Abl wt which was associated with a stabilization of the interactions between SH2-SH3 and kinase domains.

**BO1 Has the Same Affinity for MP and ATP Binding Sites.** The same protocol previously described for GNF-2 and the myristoyl group was applied on BO1, an ATP-competitive/mixed inhibitor of Abl wt.[19] The predicted binding mode revealed favorable interactions between the ligand and the MP, mainly of a hydrophobic nature (Figure 3C). The 4-fluorobenzylthio group totally fills the bottom of the pocket where it established van der Waals interactions with Ala356, Gly482, Cys483, Val487, Val525, Val527, and Leu360.

Additionally, the *p*F-phenyl ring made hydrophobic contacts with Leu359 and Leu529. A hydrogen bond was also observed between the NH of the ligand and the carbonyl backbone of Glu481. On the other hand, since BO1 acts with a mixed mechanism of action on Abl wt,[19] docking simulations have been also performed into the ATP binding site. According to its predicted binding pose, BO1 located the thiadiazole ring within the adenine region of the ATP binding site, directing the 4-fluorobenzylthio chain and the phenyl ring of the benzamido moiety toward two hydrophobic regions, labeled as hydrophobic regions I (residues Lys271, Met290, Phe382, Ile313, Val299, Val256, and Tyr253) and II (residues Leu248, Gly321, and Phe317), respectively (Figure 3D). Furthermore, BO1 was involved in two hydrogen bonds with the Met318 of the hinge region by means of the atom N4 and the NH group of the amide moiety at C5. The best docking poses of BO1 in both MP and the ATP binding sites were then used as starting points for 30 ns MD simulations. The stability of the two complexes was determined by RMSD analysis of the MD trajectories obtained from simulations with respect to the initial structure considering the C$\alpha$ of the whole complex. The results are plotted in Figure 8 down (black line for MP and green line for the ATP binding site). After 18 ns, the RMSD of C$\alpha$ tends to converge, indicating that the systems are stable and equilibrated. The MD trajectories from the last 6 ns of simulation of both systems were taken for MM-GBSA analysis. According to biological experiments for which BO1 acts against Abl wt with an ATP-competitive or mixed mechanism of action,[19] comparable binding free energy values were found for the inhibitor within MP and ATP binding sites (−33 and −36 kcal/mol, respectively, Table 4). Going into the details of interactions of the ligand into the MP, a hydrogen bond was found between the NH group of the ligand and the carbonyl backbone of Glu481 (51% occupancy). Differently from GNF-2, no hydrogen bridge involving a solvent molecule was detected for BO1. During simulation, no water molecules have been able to approach the ligand establishing a hydrogen bond. The residue decomposition of the binding free energy showed that the nonpolar contribution dominated complex interactions. The main hot spots were identified at the bottom of the hydrophobic pocket, while poor interactions were established by the ligand with the residues at the entrance of the cavity such as Arg351 and Tyr454, which were emerged as crucial for GNF-2. The binding free energy between SH2 and kinase domain after BO1 binding was −53 kcal/mol, slightly higher than those found for GNF-2 and myristoyl ligands (Table 5).

Hydrogen-bond and per-residue decomposition analysis (Tables 2-3) highlighted the same residues previously described for GNF-2 as crucial for the interaction between SH2-SH3 and kinase domains. Furthermore, time-dependent RMSF analysis of BO1 bound to the MP site was in line with the one described above for GNF-2 (Figure 9). Overall, a similar affinity of BO1 toward MP and ATP binding sites emerged from our computational studies on Abl wt. After binding to MP, BO1 resulted in being able to stabilize the compact/inhibited conformation of the enzyme similarly to that found for the GNF-2 inhibitor.

**GNF-2 and BO1 Act against the Abl T315I Mutant in a Different Way.** A different biological profile has been observed for GNF-2 and BO1 against the mutated Abl carrying the T315I mutation. GNF-2 was demonstrated to possess cellular activity against Bcr-Abl wt but failed to inhibit activity of the T315I mutant both *in vivo* and *in vitro*.[11−13] Differently, BO1 showed a peculiar biological behavior acting with an ATP-competitive or mixed mechanism of action in the case of Abl wt and as a noncompetitive inhibitor with respect to both ATP and peptide substrates on the T315I Abl mutant.[19] It remains an enigma why a potent MP binder, such as GNF-2, was unable to inhibit the gatekeeper mutant.[11−13] Structural analysis reveals that the T315I substitution promotes the active kinase conformation by the stabilization of a network of hydrophobic interactions, namely the hydrophobic spine,[34] that is a

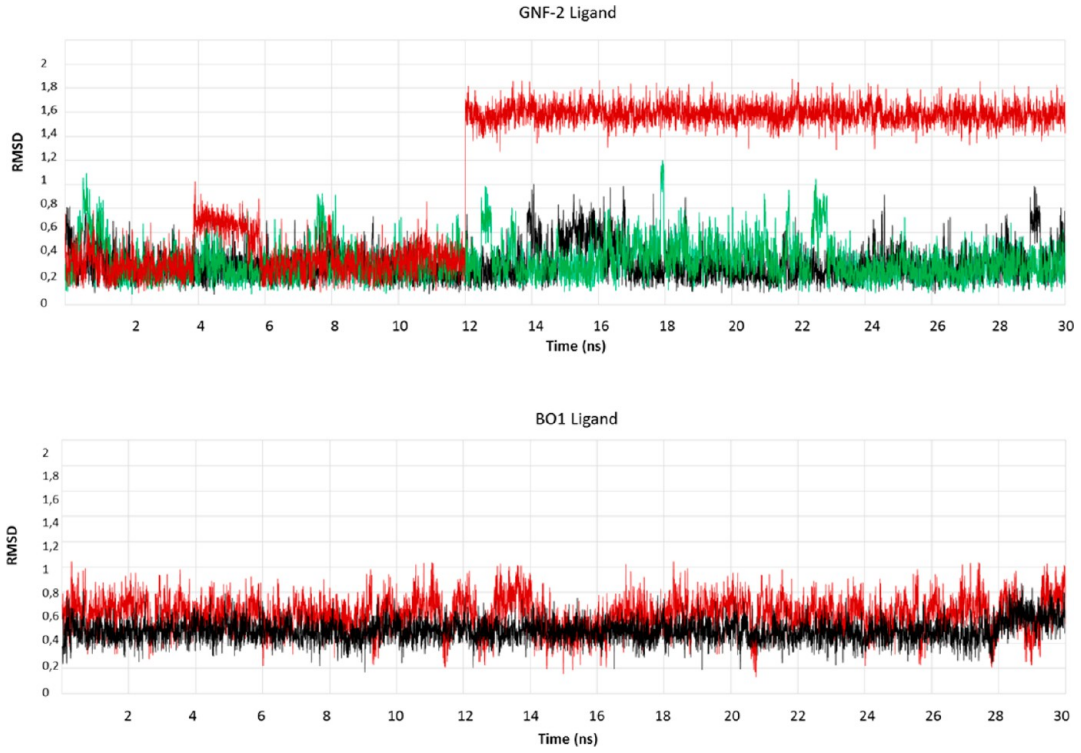


**Figure 11.** Time evolution of the RMSD values calculated on the heavy atoms of the ligand. Upper: GNF-2 bound to MP in Abl wt (black line), the T315I mutant (red line), and the T315I mutant with the concurrent binding of Imatinib within the ATP binding site (green line). Bottom: BO1 bound to MP in Abl wt (black line) and the T315I mutant (red line).

characteristic feature of the active state of several kinases. As a consequence, the stabilization of the myristoyl binding site which required a compact and inhibited conformation of the protein could be penalized in the case of the T315I mutation. Accordingly, all known allosteric Abl inhibitors were found inactive on gatekeeper mutant T315I with the only exception of BO1, the only allosteric inhibitor of gatekeeper mutant actually known. However, it has been demonstrated that some of the small molecules that target the myristate binding site such as GNF-2 are capable of inhibiting T315I Abl when used in combination with an ATP-competitive inhibitor such as Dasatinib, Nilotinib, or Imatinib.[11−13] Altogether, these results provide evidence that the binding of a small molecule to the myristate binding site induces changes to the conformational dynamics of the ATP site as revealed also by hydrogen−deuterium exchange studies.[35] In order to better understand the dynamic of the allosteric inhibition on T315I, GNF-2 and BO1 were docked within the MP of the Abl mutant, and the obtained complexes were then submitted to molecular dynamic simulations. For comparative purposes, the structure of Abl T315I was obtained by mutating the residue 315 of the Abl wt crystal structure previously used (PDB code: 1OPK) from a Thr to an Ile. Starting from the docking poses already described above for Abl wt, 30 ns MD simulations were carried out for both the complexes. Time-dependent root main square deviation (RMSD) and fluctuation (RMSF) were calculated throughout the trajectories (Figures 8-9). The binding of GNF-2 to the MP of the T315I mutant seems to have no stabilization effects on the kinase structure, indeed higher RMSF values were detected for most of the residues during the time of simulation with respect to the wt Abl complex. The larger fluctuations were observed in αE, αI, and αI′ helices (residues 468−527) as well as in the activation loop (residues 403−420) and αC-helix (residues 291−315). The terminal stage of the dynamics was used for extracting 150 snapshots and to perform the MM-GBSA analysis. With regard to the GNF-2 ligand, $\Delta G$ values displayed a weaker binding affinity to the T315I mutant than to the wt enzyme (−27.08 kcal/mol versus −38.6 kcal/mol, Table 4). Residue decomposition analysis highlighted poor interactions of GNF-2 with the amino acids that project their side chains in the MP of T315I. Interactions with residues identified as hot spots in wt such as Arg351, Leu359, Leu360, Leu448, Glu481, Val487, and Ile521 were completely lost in the binding with the T315I mutant. Surprisingly, after 12 ns of MD simulation GNF-2 partially came out from the pocket by completely changing its binding mode. Accordingly, an increased ligand RMSD was observed relative to the starting structure (Figure 11, red line). In this binding pose which was maintained by the ligand up to the end of the simulation, GNF-2 adopted a cis conformation with respect to the NH-C2 bond (Figure 12). The crucial interaction with the guanidine group of Arg351 that GNF-2 established in wt enzyme was observed only for a short time in T315I. Furthermore, no hydrogen bonds with solvent molecules were detected. Analysis of protein surface demonstrated that the pocket partially closed itself leaving insufficient space to allow the interaction of a water molecule with the ligand. A hydrogen bond with an occupancy of 15% was found between the aniline NH of GNF-2 and the side chain of Tyr454 (Figure 12). Overall, the higher flexibility of the Abl T315I mutant over the wt lead to instability in the binding of GNF-2 to MP. The low binding affinity of GNF-2 within the MP of T315I could explain its loss of activity. On the contrary, BO1 was able to keep in the T315I Abl mutant the same contacts established in the interaction with the wt enzyme. Accordingly, comparable binding free energies were found (−33.72 in wt and −32.76 in T315I).


dx.doi.org/10.1021/ci500060k | J. Chem. Inf. Model. 2014, 54, 1325−1338

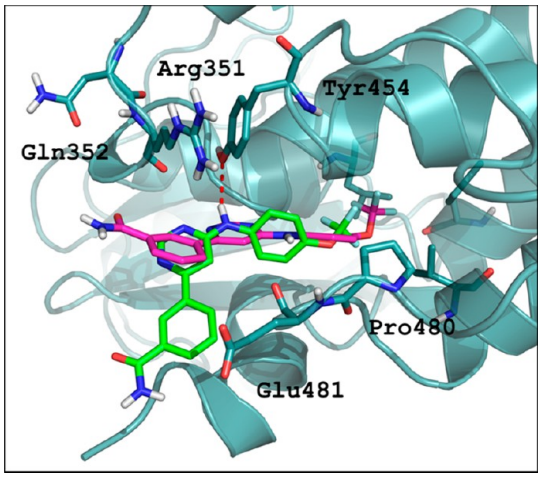


**Figure 12.** GNF-2 binding pose after 30 ns MD simulation in MP of the Abl T315I mutant (green sticks). The binding pose of GNF-2 in the last frame of MD in Abl wt was extracted and superimposed (magenta sticks).

Differently from GNF-2, BO1 maintains its binding mode for all 30 ns of MD simulation (Figure 11). The RMSF profiles of C$\alpha$ carbons in both Abl wt and T315I mutant simulations are quite similar to the only exceptions of the activation loop (403−419 residues) and the region which extends from 460 to 484 residues for which higher fluctuations were measured in the mutant complex. Because of the higher fluctuations detected in the mutated protein for residue Glu481, the stable hydrogen bond found in the wt between the ligand and the backbone carbonyl group of Glu481 occurred with a lower occupancy in T315I complex simulation (40% occupancy versus 51%). Remarkably, a stable $\pi-\pi$ interaction between the *p*-fluoro phenyl ring of BO1 and the guanidine group of Arg351 was observed during the simulation (Figure 13). BO1 was able to

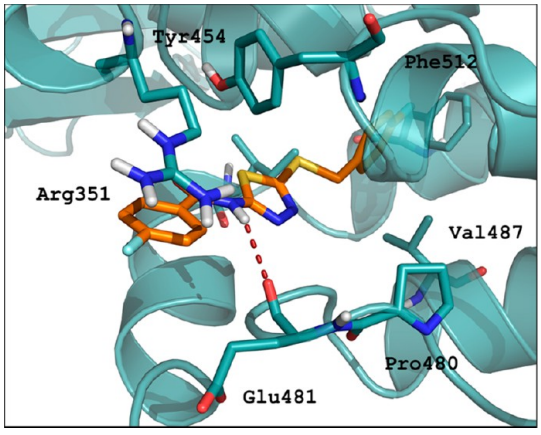


**Figure 13.** Snapshot from MD simulation of BO1 bound to MP of the Abl T315I mutant. The binding mode of the ligand is stabilized by a hydrogen bond (involving Glu481) and a $\pi-\pi$ interaction with Arg351.

stabilize much more than GNF-2 the compact/autoinhibited conformation of the T315I mutant as demonstrated by the calculation of the binding free energy between SH2-SH3 and kinase domains (−59 kcal/mol versus −42 kcal/mol). Accordingly, the effect of the two compounds on the protein dynamic is very different. BO1 stabilizes the bending of the $\alpha$I-helix assisting the docking of SH2 on kinase domain and inducing the stabilization of many interactions. The following residues were identified as hot spots: Arg189, which was involved in hydrogen bonds with Glu526 and Asp523, Tyr158, Tyr245, Tyr361, Val357, and Ser520. BO1 promoted the formation of hydrogen bonds between Asp96 and Arg282 as well as between Ser93 and Val247 which were not detected during the dynamic of GNF-2. The hydrogen bond between Glu117 and Lys313 was also stabilized. In agreement with biological data, our simulations help to elucidate the mechanism of allosteric inhibition of BO1 and GNF-2 against the T315I mutant. To summarize, GNF-2 was not able to inhibit the T315I mutant because of its inability to maintain a profitable binding mode within the pocket. While the binding of GNF-2 in Abl wt was stabilized by important polar and apolar interactions, most of these contacts were lost in T315I with the consequent instability of the enzyme compact conformation. Conversely, BO1 established favorable and stable interactions within the MP of both Abl wt and T315I, allowing the formation of the compact/inhibited conformation of the enzyme.

**GNF-2 Enhances Imatinib Activity against the T315I Mutant.** It was reported that GNF-2 could potentiate the antiproliferative activity of Imatinib on Bcr-Abl-expressing cells.[11−13] The combination of IM and GNF-2 was more effective in inhibiting Ba/F3.p210 cell growth than the ATP-competitive inhibitor alone.[11−13] Furthermore, the contemporaneous use of GNF-2 and Imatinib suppressed the emergence of resistance mutations *in vitro*, displayed additive inhibitory activity in biochemical and cellular assays against the human Bcr−Abl T315I mutant, and showed *in vivo* efficacy against the recalcitrant mutant T315I in a murine bone-marrow transplantation model. This experimental evidence demonstrated that (i) therapeutically relevant inhibition of Bcr−Abl activity can be achieved by means of inhibitors that bind to the myristate binding site and (ii) combining allosteric and ATP-competitive inhibitors it is possible to overcome resistance.[11−13] In order to investigate the synergic effect between GNF-2 and Imatinib on Abl T315I an MD simulation has been performed on the trimeric (T315I/IM/GNF-2) complex. For this purpose, we used the available crystal structure of the Abl kinase domain bound by GNF-2 and IM (PDB code 3K5V). In order to obtain the full length protein, the 3K5V structure was aligned to 1OPK, and the lacking SH2 and SH3 domains were reconstructed. Furthermore, residue Thr315 was replaced with an Ile, and the complex (kinase/IM/GNF-2) was minimized (Figure 14). The same MD protocol previously described was applied together with the MM-GBSA analysis. The affinity of GNF-2 for the MP of the T315I mutant resulted in being higher when IM is at the same time bound into the ATP binding site (−32.26 kcal/mol versus −27.08 kcal/mol). This result supports the hypothesis that the presence of IM in the ATP binding site induces a stabilization of the ligand in MP. Indeed, the binding mode of GNF-2 is maintained during all the time of simulation (Figure 11).

At the same time, Imatinib maintains its binding mode by the end of MD simulation establishing the canonical hydrogen bonds with Glu305, belonging to the $\alpha$C-helix, Asp 400, and Met318. The last frame of MD simulation is shown in Figure 14. Per residue decomposition analysis highlighted many interactions between the ligand and the receptor which were lost when GNF-2 was bound alone to the MP of the T315I mutant. Indeed, many of the hot spots identified from the MD


dx.doi.org/10.1021/ci500060k | J. Chem. Inf. Model. 2014, 54, 1325−1338

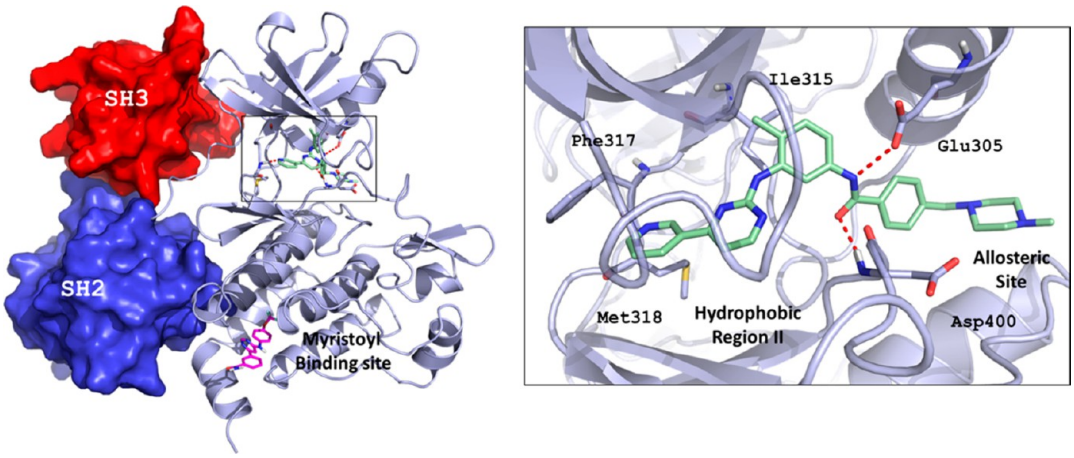


**Figure 14.** *Left*. Representation of the last frame of MD simulation of the Abl T315I mutant in which GNF-2 binds to MP and, at the same time, Imatinib occupies the ATP binding site. *Right*. Binding mode of Imatinib within the modeled active site of the T315I mutant. Imatinib binds both the ATP region and an adjacent hydrophobic pocket, namely the allosteric site. During the MD simulation GNF-2 binds to the MP and Imatinib mantains its binding mode by forming the canonical hydrogen bonds with Glu305, Asp400, and Met318.

of GNF-2 within the Abl wt were found also in this simulation. A $\pi-\pi$ interaction between the ligand and the guanidine group of Arg351 was detected at the equilibration stage which persists until the end of the simulation. Other important contacts involved Leu359, Leu360, and Glu481. The simultaneous binding of IM and GNF-2 in the ATP and MP sites, respectively, induces a stabilization effect on the compact/autoinhibited conformation of the mutated enzyme. A lower binding free energy between SH2-SH3 and kinase domains was found with respect to that calculated in the absence of IM, with an energetic advantage of about 5 kcal/mol (−47.05 kcal/mol versus −42.10 kcal/mol). The residues more involved in this little stabilization effect were Glu117, Arg194, Lys313, and Val358 (Table 3). Furthermore, a higher number of hydrogen bond interactions were found between SH2 and kinase domains in the trimeric complex (Table 3). From RMSF analysis, lower fluctuations were observed for residues of the T315I/IM/GNF-2 system than for the amino acids of the complex between Abl T315I and GNF-2. The regions more involved in this stabilization effect were the activation loop, the $\alpha$C-helix, and the $\alpha$I′-helix (Figure 8, green line). From all this analysis, the Abl T315I mutant resulted in being more stable in the case that both the catalytic and allosteric binding sites are occupied. As a consequence, it is not surprising that GNF-2 was only crystallized when IM was bound in the ATP binding site as it is known that the binding of an ATP-competitive inhibitor stabilizes the protein structure, and this aspect strongly emerged also from our studies.

## CONCLUSIONS

Owing to the resistance to ATP-competitive inhibitors in advanced CML, many efforts are underway to find new pharmacological agents that address this challenge. An approach could be the finding of new allosteric inhibitors that are able to block the kinase activity targeting pockets remotely from the ATP binding site. GNF-2 has been the first discovered allosteric Abl inhibitor. Recently, our research group identified an interesting compound, BO1, which was able to act against both Abl wt and T315I mutants with two different mechanisms of action. In the case of wt, BO1 targeted both the free enzyme and the enzyme-peptide complex, preventing ATP binding with a competitive or mixed mechanism of action; in the case of T315I BO1 acted as a noncompetitive inhibitor with respect to both ATP and a peptide substrate. Herein, molecular modeling studies were conducted on GNF-2 and BO1 to gain further insight into the allosteric inhibition mechanism of Abl wt and T315I. As a result, both inhibitors were found to form stable complexes with the inhibited conformation of Abl wt by establishing profitable interactions within the myristoyl pocket. Residues that emerged as the most important ones for the interaction within the allosteric pocket were Arg351, Leu359, Leu360, Leu448, Val487, and Ile521. Furthermore, we found that GNF-2 and BO1, through their allosteric mechanism, were able to promote the stabilization of the intramolecular interactions which occur between SH2-SH3 and kinase domains as suggested by the free energy of binding calculated between the interacting regions. The identification of residues critical for the correct positioning of the SH2-SH3 and kinase domains in the compact/autoinhibited conformation, namely hotspots, was thus performed. A $\pi-\pi$ interaction between Tyr158 and Tyr361 was recurrent in our analysis confirming its importance. The low binding energy associated with both Tyr158 and Tyr361 in residue decomposition analysis demonstrated how these amino acids are fundamental for the proper localization of SH2 onto catalytic domain. Similarly, Arg189, which was involved in forming stable hydrogen bonds with Glu526 and Asp523 (both belonging to the catalytic domain), was recognized as a crucial hot spot because of its significant energetic contribution to the stabilization of SH2-kinase domain interaction. On the other hand, in agreement with experimental studies, we observed a different effect of the two inhibitors against the mutant T315I. In particular, the efficiency of GNF-2 in stabilizing the interactions between SH2-SH3 and kinase domains was strongly reduced when Thr315 was mutated into Ile within the ATP binding site. This single mutation seems to be able to completely destabilize the binding mode of GNF-2 which comes partially out from the pocket by changing its pose during the simulation. On the contrary, BO1 was found able to deeply stabilize the compact/inhibited conformation of Abl T315I because of its ability to maintain profitable interactions also in MP of the mutated enzyme. In line with experimental evidence, a synergistic effect of GNF-2 and Imatinib in the stabilization of the closed conformation was also observed.

In general, we found that the T315I mutation was able to alter the dynamics properties of the whole protein, and in the case of the GNF-2 ligand the instability of the system causes the partial ligand escape from the binding site. Overall, results here reported could help the design of novel allosteric inhibitors.

## AUTHOR INFORMATION


### Corresponding Author

*Phone: +39 0577 234306. Fax: +39 0577 234306. E-mail: botta.maurizio@gmail.com. Corresponding author address: Dipartimento di Biotecnologie Chimica e Farmacia, Università degli Studi di Siena, Via Aldo Moro, 2, 53100 Siena, Italy.


### Notes

The authors declare no competing financial interest.

## ACKNOWLEDGMENTS

This work was partially supported by the Istituto Toscano Tumori-ITT-Grant proposal 2010. S.S. was also supported by the National Interest Research Project PRIN_2010_5YY2HL. We are grateful to Lead Discovery Siena Srl and Cost Action CM1106 "Chemical Approaches to Targeting Drug Resistance in Cancer Stem Cells". We are indebted to Molecular Discovery for access to the GRID code.

## REFERENCES


(1) Hantschel, O.; Superti-Furga, G. Regulation of the c-Abl and Bcr-Abl tyrosine kinases. *Nat. Rev. Mol. Cell. Biol.* **2004**, *5*, 33−44.

(2) Deininger, M.; Buchdunger, E.; Druker, B. J. The development of imatinib as a therapeutic agent for chronic myeloid leukemia. *Blood* **2005**, *105*, 2640−2653.

(3) Jabbour, E.; Kantarjian, H. Chronic myeloid leukemia: 2012 update on diagnosis, monitoring, and management. *Am. J. Hematol.* **2012**, *87*, 1037−1045.

(4) O'Hare, T.; Eide, C. A.; Deininger, M. W. New Bcr-Abl inhibitors in chronic myeloid leukemia: keeping resistance in check. *Expert Opin. Invest. Drugs.* **2008**, *17*, 865−878.

(5) Schenone, S.; Brullo, C.; Botta, M. New opportunities to treat the T315I-Bcr-Abl mutant in chronic myeloid leukaemia: tyrosine kinase inhibitors and molecules that act by alternative mechanisms. *Curr. Med. Chem.* **2010**, *17*, 1220−1245.

(6) Burgess, M. R.; Skaggs, B. J.; Shah, N. P.; Lee, F. Y.; Sawyers, C. L. Comparative analysis of two clinically active BCR-ABL kinase inhibitors reveals the role of conformation-specific binding in resistance. *Proc. Natl. Acad. Sci. U. S. A.* **2005**, *102*, 3395−3400.

(7) O'Hare, T.; Pollock, R.; Stoffregen, E. P.; Keats, J. A.; Abdullah, O. M.; Moseson, E. M.; Rivera, V. M.; Tang, H.; Metcalf, C. A., III; Bohacek, R. S.; Wang, Y.; Sundaramoorthi, R.; Shakespeare, W. C.; Dalgarno, D.; Clackson, T.; Sawyer, T. K.; Michael, W.; Deininger, M. W.; Druker, B. J. Inhibition of wild-type and mutant Bcr-Abl by AP23464, a potent ATP-based oncogenic protein kinase inhibitor: implications for CML. *Blood* **2004**, *104*, 2532−2539.

(8) Huron, D. R.; Gorre, M. E.; Kraker, A. J.; Sawyers, C. L.; Rosen, N.; Moasser, M. M. A novel pyridopyrimidine inhibitor of abl kinase is a picomolar inhibitor of Bcr-abl-driven K562 cells and is effective against STI571-resistant Bcr-Abl mutants. *Clin. Cancer Res.* **2003**, *9*, 1267−1273.

(9) Nagar, B.; Hantschel, O.; Young, M. A.; Scheffzek, K.; Veach, D.; Bornmann, W.; Clarkson, B.; Superti-Furga, G.; Kuriyan, J. Structural Basis for the Autoinhibition of c-Abl Tyrosine Kinase. *Cell* **2003**, *112*, 859−871.

(10) Hantschel, O.; Nagar, B.; Guettler, S.; Kretzschmar, J.; Dorey, K.; Kuriyan, J.; Superti-Furga, G. A. Myristoyl/Phosphotyrosine Switch Regulates c-Abl. *Cell* **2003**, *112*, 845−857.

(11) Iacob, R. E.; Zhang, J.; Gray, N. S.; Engen, J. R. Allosteric interaction between the myristate and ATP site of abl kinase. *PLoS One* **2011**, *6*, e15929.

(12) Khateb, M.; Ruimi, N.; Khamisie, H.; Najajreh, Y.; Mian, A.; Metodieva, A.; Ruthardt, M.; Mahajna, J. Overcoming Bcr-Abl mutation by combination of GNF-2 and ATP competitors in an Abl-independent mechanism. *BMC Cancer* **2012**, *12*, 563.

(13) Zhang, J.; Adrián, F. J.; Jahnke, W.; Cowan-Jacob, S. W.; Li, A. G.; Iacob, R. E.; Sim, T.; Powers, J.; Dierks, C.; Sun, F.; Guo, G. R.; Ding, O.; Okram, B.; Choi, Y.; Wojciechowski, A.; Deng, X.; Liu, G.; Fendrich, G.; Strauss, A.; Vajpai, N.; Grzesiek, S.; Tuntland, T.; Liu, Y.; Bursulaya, B.; Azam, M.; Manley, P. W.; Engen, J. R.; Daley, G. Q.; Warmuth, M.; Gray, N. S. Targeting Bcr−Abl by combining allosteric with ATP-binding-site inhibitors. *Nature* **2010**, *463*, 501−506.

(14) Adrian, F. J.; Ding, Q.; Sim, T.; Velentza, A.; Sloan, C.; Liu, Y.; Zhang, G.; Hur, W.; Ding, S.; Manley, P.; Mestan, J.; Fabbro, D.; Gray, N. S. Allosteric inhibitors of Bcr-Abl dependent cell proliferation. *Nat. Chem. Biol.* **2006**, *2*, 95−102.

(15) Deng, X.; Okram, B.; Ding, Q.; Zhang, J.; Choi, Y.; Adrián, F. J.; Wojciechowski, A.; Zhang, G.; Che, J.; Bursulaya, B.; Cowan-Jacob, S. W.; Rummel, G.; Sim, T.; Gray, N. S. Expanding the Diversity of Allosteric Bcr-Abl Inhibitors. *J. Med. Chem.* **2010**, *53*, 6934−6946.

(16) Jahnke, W.; Grotzfeld, R. M.; Pellé, X.; Strauss, A.; Fendrich, G.; Cowan-Jacob, S. W.; Cotesta, S.; Fabbro, D.; Furet, P.; Mestan, J.; Marzinzik, A. L. Binding or bending: distinction of allosteric Abl kinase agonists from antagonists by an NMR-based conformational assay. *J. Am. Chem. Soc.* **2010**, *132*, 7043−7048.

(17) Yang, J.; Campobasso, N.; Biju, M. P.; Fisher, K.; Pan, X. Q.; Cottom, J.; Galbraith, S.; Ho, T.; Zhang, H.; Hong, X.; Ward, P.; Hofmann, G.; Siegfried, B.; Zappacosta, F.; Washio, Y.; Cao, P.; Qu, J.; Bertrand, S.; Wang, D. Y.; Head, M. S.; Li, H.; Moores, S.; Lai, Z.; Johanson, K.; Burton, G.; Erickson-Miller, C.; Simpson, G.; Tummino, P.; Copeland, R. A.; Oliff, A. Discovery and characterization of a cell-permeable, small molecule c-Abl activator that binds to the myristoyl binding site. *Chem. Biol.* **2011**, *18*, 177−186.

(18) Schneider, R.; Becker, C.; Simard, J. R.; Getlik, M.; Bohlke, N.; Janning, P.; Rauh, D. Direct Binding assay for the Detection of Type IV Allosteric Inhibitors of Abl. *J. Am. Chem. Soc.* **2012**, *134*, 9138−9141.

(19) (a) Radi, M.; Crespan, E.; Botta, G.; Falchi, F.; Maga, G.; Manetti, F.; Corradi, V.; Mancini, M.; Santucci, M. A.; Schenone, S.; Botta, M. Discovery and SAR of 1,3,4-thiadiazole derivatives as potent Abl Tyrosine Kinase inhibitors and cytodifferentiating agents. *Bioorg. Med. Chem. Lett.* **2008**, *18*, 1207−1211. (b) Radi, M.; Crespan, E.; Falchi, F.; Bernardo, V.; Zanoli, S.; Manetti, F.; Schenone, S.; Maga, G.; Botta, M. Design and Synthesis of Thiadiazoles and Thiazoles Targeting the Bcr-Abl T315I Mutant: from Docking False Positive to ATP-Noncompetitive Inhibitors. *ChemMedChem.* **2010**, *5*, 1226−1231. (c) Crespan, E.; Radi, M.; Zanoli, S.; Schenone, S.; Botta, M.; Maga, G. Dual SRC and ABL inhibitors target wild type ABL and the ABLT315I imatinib-resistant mutant with different mechanisms. *Bioorg. Med. Chem.* **2010**, *18*, 3999−4008.

(20) Karplus, M.; Petsko, G. A. Molecular dynamics simulations in biology. *Nature* **1990**, *347*, 631−639.

(21) Kollman, P. A.; Massova, I.; Reyes, C.; Kuhn, B.; Huo, S.; Chong, L.; Lee, M.; Lee, T.; Duan, Y.; Wang, W.; Donini, O.; Cieplak, P.; Srinivasan, J.; Case, D. A.; Cheatham, T. Calculating structures and free energies of complex molecules: combining molecular mechanics and continuum models. *Acc. Chem. Res.* **2000**, *33*, 889−897.

(22) Gohlke, H.; Kiel, C.; Case, D. A. Insight into protein-protein binding by binding free energy calculation and free energy decomposition for the Ras-Raf and Ras-RalGDS complexes. *J. Mol. Biol.* **2003**, *330*, 891−913.

(23) Schrödinger Suite 2011 Protein Preparation Wizard; *Epik* version 2.2; Schrödinger, LLC: New York, 2011. *Impact* version 5.7; Schrödinger, LLC: New York, 2011. *Prime* version 3.0; Schrödinger, LLC: New York, 2011.

(24) *Maestro*, version 9.2; Schrödinger, LLC: New York, 2011.

(25) *MacroModel*, version 9.9; Schrödinger, LLC: New York, 2011.

(26) *LigPrep*, version 2.5; Schrödinger, LLC: New York, 2011.

(27) *Glide*, version 5.7; Schrödinger, LLC: New York, 2011. Friesner, R. A.; Banks, J. L.; Halgren, T. A.; Klicic, J. J.; Mainz, D. T.; Repasky,

M. P.; Knoll, E. H.; Shaw, D. E.; Shelley, M.; Perry, J. K.; Francis, P.; Shenkin, P. S. Glide: a new approach for rapid, accurate docking and scoring. 1. Method and assessment of docking accuracy. *J. Med. Chem.* **2004**, *47*, 1739−1749.
(28) Tintori, C.; Veljkovic, N.; Veljkovic, V.; Botta, M. Computational studies of the interaction between the HIV-1 integrase tetramer and the cofactor LEDGF/p75: insights from molecular dynamics simulations and the informational spectrum method. *Proteins* **2010**, *78*, 3396−3408.
(29) Wang, J.; Wolf, R. M.; Caldwell, J. W.; Kollman, P. A.; Case, D. A. Development and testing of a general AMBER force field. *J. Comput. Chem.* **2004**, *25*, 1157−1174.
(30) Wang, J.; Wang, W.; Kollman, P. A.; Case, D. A. Automatic atom type and bond type perception in molecular mechanical calculations. *J. Mol. Graphics Modell.* **2006**, *25*, 247−260.
(31) Rocchia, W.; Alexov, E.; Honig, B. Extending the applicability of non linear Poisson-Boltzmann equation: Multiple dielettric constant and multivalent ions. *J. Phys. Chem. B* **2001**, *105*, 6507−6514.
(32) Onufriev, A.; Bashford, D.; Case, D. A. Exploring protein native states and large-scale conformational changes with a modified generalized born model. *Proteins* **2004**, *55*, 383−394.
(33) *Grid*, version 22; Molecular Discovery Ltd.: Pinner, Middlesex, U.K.
(34) Azam, M.; Seeliger, M. A.; Gray, N. S.; Kuriyan, J.; Daley, G. Q. Activation of tyrosine kinases by mutation of the gatekeeper threonine. *Nat. Struct. Mol. Biol.* **2008**, *15*, 1109−1118.
(35) Iacob, R. E.; Pene-Dumitrescu, T.; Zhang, J.; Gray, N. S.; Smithgall, T. E.; Engen, J. R. Conformational disturbance in Abl kinase upon mutation and deregulation. *Proc. Nat. Acad. Sci.* **2009**, *106*, 1386−1391.